Applied Ocean Research 117 (2021) 102947

Contents lists available at ScienceDirect

Applied Ocean Research

journal homepage: www.elsevier.com/locate/apor

An experimental study of adaptive bounded depth control for underwater vehicles subject to thruster's dead-zone and saturation

Caoyang Yu [a,b,c], Yiming Zhong [a], Lian Lian [a,c,*], Xianbo Xiang [d]

[a] School of Oceanography, Shanghai Jiao Tong University, Shanghai 200030, China
[b] Key Laboratory of Marine Environmental Survey Technology and Application, Ministry of Natural Resources, China
[c] State Key Laboratory of Ocean Engineering, Shanghai Jiao Tong University, Shanghai 200240, China
[d] School of Naval Architecture and Ocean Engineering, Huazhong University of Science and Technology, Wuhan 430074, China

ARTICLE INFO

Keywords:
Underwater vehicle
Depth control
Dead-zone compensation
Input saturation

ABSTRACT

Accurate depth tracking control is of great importance for an underwater vehicle that performs an underwater task such as seabed mapping and underwater docking. This paper addresses the problem of adaptive depth tracking control for an underwater vehicle, particularly in the presence of hydrodynamics uncertainty, thruster's dead-zone and saturation. Before deriving an adaptive depth control law, an unified and continuous hydrodynamics model in heave is built, where the thruster's characteristics composed of output time-delay, input dead-zone and saturation are taken into consideration. Subsequently, fuzzy universal approximation theorem is resorted to online approximate the unknown and complex hydrodynamics in heave, and then adaptive sliding mode control technique is utilized to compensate for the approximation residual. In order to reject inherent input saturation, gradient projection method is introduced into the above adaptive control law, resulting in an adaptive bounded depth control law. Furthermore, through obtaining two dead-zone breakpoints in advance and online translation compensation, the final control output can always change within the permitted range. Finally, three comparative experiments are performed to verify the outperformance of the designed adaptive bounded depth tracking controller.

1. Introduction

In recent decades, dynamics modeling and motion control of ocean vehicles have attracted extensive attention from oceanic research groups (Fossen, 2011; Wang and Li, 2020; Wang et al., 2021). Examples of motion control include maneuvering control, setpoint regulation, trajectory tracking and path following Fossen (2011), Shojaei and Chatraei (2021) and Peng and Wang (2018). Among them, depth control in heave dynamics is one of the low-level basic control missions for underwater vehicles and plays a crucial role in seabed mapping, underwater docking and so on (Healey and Lienard, 1993; Lapierre, 2009; Li et al., 2015).

Various advanced controllers have been designed and utilized to address the problem of underwater depth tracking. In Tanakitkorn et al. (2017), a proportion integral minus differential (PI-D) based controller is developed to maintain depth of the Delphin 2 system. In this PI-D control, an actual depth state of the underwater system is fed to the derivative term instead of the tracking error, which avoids the setpoint kick phenomenon in the conventional proportion–integral–differential (PID) control, i.e., a sudden step change in the required depth state. In Maalouf et al. (2015), an L_1 adaptive controller with decoupled robustness and adaptation is applied to complete depth control of a micro remotely operated vehicle called AC-ROV. The proposed control architecture shows a faster performance in adaptation compared to the well-known adaptive nonlinear state feedback controller. Depth holding and profile tracking experiments of an autonomous diving agent are carried out to verify the effectiveness of the designed feedback linearization controller enhanced by an adaptive fuzzy approximation to cope with modeling uncertainties (Solowjow et al., 2017). Similarly, to achieve robust diving control of an autonomous underwater vehicle, an online neural network estimator combined with corrective control based on an adaptive fuzzy proportional–integral control law is proposed in Lakhekar et al. (2020).

It can be observed that the above research does not consider thruster's saturation of underwater vehicles. In fact, this inherent characteristic maybe cause performance degradation or even instability in the closed-loop response of tracking systems (Cui et al., 2017; Yu et al., 2020). To solve this problem, a slack variable is first introduced in Naik and Singh (2007) to transform the saturated rudder

* Corresponding author at: School of Oceanography, Shanghai Jiao Tong University, Shanghai 200030, China.
E-mail addresses: yucaoyang@sjtu.edu.cn (C. Yu), eduzhongym@sjtu.edu.cn (Y. Zhong), llian@sjtu.edu.cn (L. Lian), xbxiang@hust.edu.cn (X. Xiang).

https://doi.org/10.1016/j.apor.2021.102947
Received 1 June 2021; Received in revised form 26 August 2021; Accepted 25 October 2021
Available online 23 November 2021

control problem into an unsaturated problem. Subsequently, the state-dependent Riccati equation technique is resorted to achieve suboptimal dive plane control of the Remote Environmental Monitoring UnitS (REMUS). In Chu et al. (2018), a new modified auxiliary system with time-varying nonlinear gains is proposed to compensate for the effects of input saturation in diving control of underwater vehicles as well as to remove the assumption regarding bounded auxiliary states. In Wu et al. (2018), augment L_1 adaptive control with Riccati-based anti-windup compensator is utilized to modify the pitch tracking performance of REMUS in the presence of saturation. In Yu et al. (2018), an adaptive fuzzy control system based on universal approximation theorem is employed to compensate for the difference between the unconstrained actuator output and the constrained one, such that the final adaptive control law can guarantee the convergence of all the tracking errors in the vertical plane. Different from Yu et al. (2018), a novel saturated kinetic control scheme is proposed to reject unknown bound of actuator saturation (Zhang et al., 2021). In Sedghi et al. (2021), adaptive robust nonlinear control is designed in the presence of unknown saturation nonlinearities generated by the physical constraints of underwater vehicle's actuators.

In fact, there also exists dead-zone characteristic in underwater thrusters, which indicates the corresponding resulting thrust in dead-zone is zero in spite of nonzero command acting on thrusters. In Chu et al. (2017), simulation results show this characteristic will cause the chattering of motion tracking and moment inputs of underwater vehicles. The vectorial configuration of thrusters is exploited in Ropars et al. (2018) in order to remove the effects of dead-zone in yaw control of a remotely operated vehicle. In Xia et al. (2015), a fuzzy logic-based dead-zone compensator is resorted to cope with the unknown dead-zone characteristic of actuators in dynamic positioning of underwater vehicles. An adaptive dead zone compensator based on fuzzy rules is built in Chen et al. (2019) to eliminate the negative effect of dead-zone on the actuators of underwater vehicles.

To the best of our knowledge, few studies consider thruster's dead-zone and saturation in the diving control of underwater vehicles simultaneously. Motivated by this consideration, this papers aims to propose an adaptive and bounded control law to achieve the depth tracking of underwater vehicles in the presence of thruster's dead-zone and saturation. In addition, hydrodynamics uncertainty and thruster's time-delay dynamics are taken into consideration in depth control.

The rest of this paper is organized as follows. Depth dynamics modeling of underwater vehicles considering thruster's time-delay, dead-zone and saturation is presented in the next section. In Section 3, the designed adaptive bounded depth control law and its stability analysis are subsequently described. Comparative experimental results are given in Section 4. Conclusion and future work are summarized in Section 5.

2. Motion modeling of underwater vehicles

2.1. Generalized modeling

Let $\{I\}$ be the earth-fixed frame and $\{B\}$ be the body-fixed frame, as shown in Fig. 1. Based on this, $\boldsymbol{\eta} = [x, y, z, \phi, \theta, \psi]^T$ expresses the position and attitude of underwater vehicles in frame $\{I\}$ and $\boldsymbol{\upsilon} = [u, v, w, p, q, r]^T$ denotes the linear and angular velocity vector in frame $\{B\}$. Referring to Fossen (1994), motion equations of underwater vehicles can be composed of

$$\dot{\boldsymbol{\eta}} = \boldsymbol{J}(\boldsymbol{\eta})\boldsymbol{\upsilon} \tag{1}$$

and

$$\boldsymbol{M}\dot{\boldsymbol{\upsilon}} = -\boldsymbol{C}(\boldsymbol{\upsilon})\boldsymbol{\upsilon} - \boldsymbol{D}(\boldsymbol{\upsilon})\boldsymbol{\upsilon} - \boldsymbol{g}(\boldsymbol{\eta}) + \boldsymbol{\tau} + \boldsymbol{J}^{-1}(\boldsymbol{\eta})\boldsymbol{\tau}_E \tag{2}$$

where they denote the kinematics and dynamics equations, respectively. Among them, $\boldsymbol{J}(\boldsymbol{\eta})$ is a transformation matrix, $\boldsymbol{M}$ denotes the inertia matrix including added mass, $\boldsymbol{C}(\boldsymbol{\upsilon})$ denotes the matrix of Coriolis and centripetal terms, $\boldsymbol{D}(\boldsymbol{\upsilon})$ denotes the damping matrix, $\boldsymbol{g}(\boldsymbol{\eta})$ denotes the vector of gravitational forces and moments, $\boldsymbol{\tau}$ denotes the vector of thruster outputs in frame $\{B\}$, and $\boldsymbol{\tau}_E$ denotes the environmental disturbances in frame $\{I\}$.

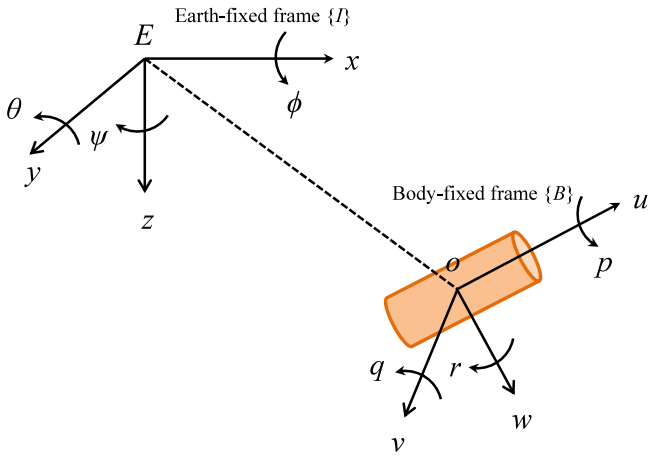

Fig. 1. Frame definition for underwater vehicles.

Substituting (1) into (2) leads to

$$\boldsymbol{M}^*(\boldsymbol{\eta})\ddot{\boldsymbol{\eta}} = -\boldsymbol{C}^*(\boldsymbol{\nu}, \boldsymbol{\eta})\dot{\boldsymbol{\eta}} - \boldsymbol{D}^*(\boldsymbol{\nu}, \boldsymbol{\eta})\dot{\boldsymbol{\eta}} - \boldsymbol{J}^{-T}\boldsymbol{g}(\boldsymbol{\eta}) + \boldsymbol{J}^{-T}(\boldsymbol{\eta})\boldsymbol{\tau} + \boldsymbol{J}^{-T}\boldsymbol{J}^{-1}\boldsymbol{\tau}_E \tag{3}$$

with

$$\begin{cases} \boldsymbol{M}^*(\boldsymbol{\eta}) = \boldsymbol{J}^{-T}(\boldsymbol{\eta})\boldsymbol{M}\boldsymbol{J}^{-1}(\boldsymbol{\eta}) \\ \boldsymbol{C}^*(\boldsymbol{\nu}, \boldsymbol{\eta}) = \boldsymbol{J}^{-T}(\boldsymbol{\eta})[\boldsymbol{C}(\boldsymbol{\upsilon}) - \boldsymbol{M}\boldsymbol{J}^{-1}(\boldsymbol{\eta})\dot{\boldsymbol{J}}(\boldsymbol{\eta})]\boldsymbol{J}^{-1}(\boldsymbol{\eta}) \\ \boldsymbol{D}^*(\boldsymbol{\nu}, \boldsymbol{\eta}) = \boldsymbol{J}^{-T}(\boldsymbol{\eta})\boldsymbol{D}(\boldsymbol{\upsilon})\boldsymbol{J}^{-1}(\boldsymbol{\eta}) \end{cases} \tag{4}$$

It is well known that each underwater vehicle has six degrees of freedom including surge, sway, heave, roll, pitch and yaw. Therefore, there are six equations after expanding (3). For the depth control mission for an underwater vehicle, the third equation in (3) can be rewritten as follows:

$$m_{33}\ddot{z} = -c_{33}(\dot{z})\dot{z} - d_{33}(\dot{z})\dot{z} - g_3(z) + h_{3i} + \tau_3 + \tau_{e3} \tag{5}$$

where z denotes its depth, h_{3i} denotes the coupling effect of heave and the other five degrees of freedom, the variable $(\cdot)_3$ denotes the third element of the corresponding vector, and the variable $(\cdot)_{33}$ denotes the element in the third row and the third column of the corresponding matrix.

Remark 1. Although some advanced numerical and experimental methods have been developed to measure the force of underwater vehicles, it is almost impossible to obtain the real-time accurate hydrodynamic coefficients, i.e., m_{33}, c_{33}, d_{33}, h_{3i} and g_3. In addition, it is noted that the inertia mass m_{33} satisfies $m_{33} > 0$.

Remark 2. The state variable z is measurable because underwater vehicles are usually equipped with the depth gauge. Further, $\dot{z}$ and $\ddot{z}$ can be approximated based on difference operation.

Assumption 1 (*Zhang et al., 2021; Do, 2016*)**.** The environmental disturbance τ_{e3} in heave is assumed to be bounded but unknown. In addition, it is slowly changing, which means its derivative $\dot{\tau}_{e3}$ is also bounded.

2.2. Thruster time constant

Let $\alpha > 0$ be the time constant of thrusters in heave and then the corresponding thrust time-delay dynamics equation can be given by

$$\alpha\dot{\tau}_3 + \tau_3 = \tau_{3c} \tag{6}$$

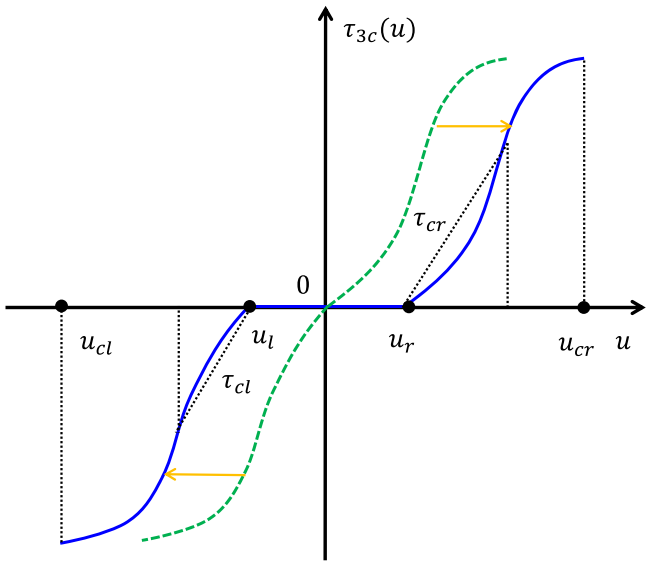

Fig. 2. Thruster's dead-zone and saturation model.

where τ_3 and τ_{3c} denote the current thrust state and thrust command in heave, respectively (Fossen and Berge).

Substituting (6) into (5) yields

$$m_{33}\alpha\ddot{z} = f(z,\dot{z},\ddot{z}) + d + \tau_{3c} \tag{7}$$

with

$$\begin{cases} f(z,\dot{z},\ddot{z}) = \begin{array}{l} -[\alpha c_{33}(\dot{z}) + \alpha d_{33}(\dot{z}) + m_{33}]\ddot{z} \\ -[\alpha\dot{c}_{33}(\dot{z}) + c_{33}(\dot{z}) + \alpha\dot{d}_{33}(\dot{z}) + d_{33}(\dot{z})]\dot{z} \\ -\alpha\dot{g}_3(z) - g_3(z) \end{array} \\ d = \alpha\dot{h}_{3i} + \alpha\dot{\tau}_{e3} + h_{3i} + \tau_{e3} \end{cases} \tag{8}$$

Remark 3. It is well known that the motion of underwater vehicles is relatively slow due to the inertia and the surrounding fluid. Combining this fact with Assumption 1 yields that d is bounded but complex and unknown.

2.3. Thruster dead-zone

In addition to the time constant, there exists a narrow dead-zone in the neighborhood of zero command for each thruster, namely, in spite of nonzero command and energy consumption acting on thrusters, the corresponding resulting force $\tau_{3c}(u) = 0$ for $u \in [u_l, u_r]$, where u denotes the command input of thrusters and $[u_l, u_r]$ is the dead-zone of thrusters, as shown in Fig. 2.

Considering the dead-zone, the relationship between the thrust command and its control command can be described by (Wang et al., 2004)

$$\tau_{3c} = \begin{cases} \tau_{cr}(u)(u - u_r), & \text{for } u \geq u_r, \\ 0, & \text{for } u_l < u < u_r, \\ \tau_{cl}(u)(u - u_l), & \text{for } u \leq u_l, \end{cases} \tag{9}$$

Assumption 2 (*Chu et al., 2017*)**.** As shown in Fig. 2, the slopes τ_{cr}, τ_{cl} in positive and negative regions outside of dead-zone are time-varying and unknown, but they and their derivatives are assumed to be positive and bounded, namely, $0 < \tau_{cr}(u) \leq \tau_{crm}$, $0 < \dot{\tau}_{cr}(u) \leq d\tau_{crm}$ for all u and $0 < \tau_{cl}(u) \leq \tau_{clm}$, $0 < \dot{\tau}_{cl}(u) \leq d\tau_{clm}$ for all u, where τ_{clm}, $d\tau_{clm}$, τ_{crm}, and $d\tau_{crm}$ are positive constants.

From a practical point of view, (9) can be rewritten as

$$\tau_{3c}(u) = \boldsymbol{\Gamma}^T(u)\boldsymbol{\Phi}(u)u + \rho(u) \tag{10}$$

where

$$\boldsymbol{\Gamma}(u) = [\tau_{cr}(u), \tau_{cl}(u)]^T \tag{11}$$

$$\boldsymbol{\Phi}(u) = [\varphi_r(u), \varphi_l(u)]^T \tag{12}$$

$$\varphi_r(u) = \begin{cases} 1, \text{ for } u \geq u_l, \\ 0, \text{ for } u < u_l, \end{cases} \tag{13}$$

$$\varphi_l(u) = \begin{cases} 0, \text{ for } u \geq u_r, \\ 1, \text{ for } u < u_r, \end{cases} \tag{14}$$

and

$$\rho(u) = \begin{cases} -\tau_{cr}(u)u_r, & \text{for } u \geq u_r, \\ -[\tau_{cl}(u) + \tau_{cr}(u)]u, & \text{for } u_l < u < u_r, \\ -\tau_{cl}(u)u_l, & \text{for } u \leq u_l, \end{cases} \tag{15}$$

Remark 4. From Assumption 2, it can be also concluded that $\rho(u)$ is bounded and satisfies $-(\tau_{clm} + \tau_{crm})u_r \leq \rho(u) \leq -(\tau_{clm} + \tau_{crm})u_l$.

2.4. Thruster saturation

It is well known that there exists inherent input saturation for each thruster. Therefore, the control input command of thrusters should be bounded, namely,

$$u = \text{sat}(u_c) \tag{16}$$

where u_c is the output command from the designed depth controller and $\text{sat}(u_c)$ is defined as

$$\text{sat}(u_c) = \begin{cases} u_{cr}, & \text{for } u_c \geq u_{cr}, \\ u_c, & \text{for } u_{cl} < u_c < u_{cr}, \\ u_{cl}, & \text{for } u_c \leq u_{cl}, \end{cases} \tag{17}$$

with u_{cr} and u_{cl} being the permitted upper bound and lower bound, as shown in Fig. 2.

Define the saturation error δ as

$$\delta = u - u_c \tag{18}$$

Substituting (10) and (18) into (7), we can rewrite the depth dynamics equation in the following form

$$m_{33}\alpha\ddot{z} = f(z,\dot{z},\ddot{z}) + \boldsymbol{\Gamma}^T(u)\boldsymbol{\Phi}(u)\delta + d + \rho(u) + \boldsymbol{\Gamma}^T(u)\boldsymbol{\Phi}(u)u_c \tag{19}$$

3. Adaptive bounded depth control

3.1. Controller design

The control objective of this paper is to make an underwater vehicle converge to and follow a predefined depth z_d. To achieve this control objective, an adaptive bounded depth control system is proposed in Fig. 3, where a fuzzy universal approximator is utilized to reject the system uncertainty and an adaptive sliding mode control law removes the effort of the fuzzy approximation error. It should be noted that gradient projection method is resorted to guarantee the boundedness of all the adaptive parameters and the translation compensation avoids the dead-zone phenomenon.

First, a time-varying sliding surface s with respect to the depth error $\tilde{z}$ is defined as

$$s = (\frac{\mathrm{d}}{\mathrm{d}t} + \lambda)^{n-1}\tilde{z} \tag{20}$$

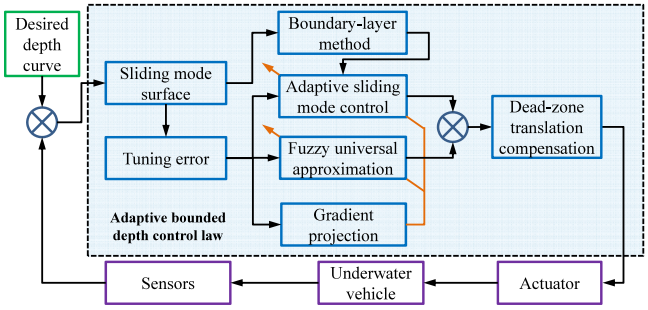

Fig. 3. Block diagram of the proposed adaptive bound depth control system.

where t is the time, λ is a positive constant, n denotes the order of the dynamic system (19) and the depth error $\tilde{z}$ is

$$\tilde{z} = z - z_d \tag{21}$$

From (20) and (21) and taking $n = 3$, it follows

$$s = \dddot{\tilde{z}} + 2\lambda\ddot{\tilde{z}} + \lambda^2\dot{\tilde{z}} \tag{22}$$

According to (19), we then have

$$\begin{aligned}\dot{s} &= \dddot{\tilde{z}} + 2\lambda\ddot{\tilde{z}} + \lambda^2\dot{\tilde{z}} \\ &= \underbrace{\frac{\boldsymbol{\Gamma}^T(u)\boldsymbol{\Phi}(u)}{\alpha m_{33}}}_{K}[\underbrace{\frac{f(z,\dot{z},\ddot{z}) - \alpha m_{33}\ddot{z}_d + 2\alpha m_{33}\lambda\ddot{\tilde{z}} + \alpha m_{33}\lambda^2\dot{\tilde{z}}}{\boldsymbol{\Gamma}^T(u)\boldsymbol{\Phi}(u)}}_{F} \\ &+ \underbrace{\frac{d+\rho(u)}{\boldsymbol{\Gamma}^T(u)\boldsymbol{\Phi}(u)}}_{D} + \delta + u_c]\end{aligned} \tag{23}$$

Remark 5. Combining (11) with (12), it follows that $\boldsymbol{\Gamma}^T(u)\boldsymbol{\Phi}(u) = \tau_{cr}(u)\varphi_r(u) + \tau_{cl}(u)\varphi_l(u) = \begin{cases}\tau_{cr}(u), & \text{for } u \geq u_l \\ \tau_{cl}(u) + \tau_{cr}(u), & \text{for } u_r < u < u_l \\ \tau_{cl}(u), & \text{for } u \leq u_r\end{cases}$, which satisfies $0 < \boldsymbol{\Gamma}^T(u)\boldsymbol{\Phi}(u) \leq \tau_{clm} + \tau_{crm}$ according to Assumption 2. Therefore, (23) is non-singular in the whole region. In addition, K, F, and D are unknown, but F is a function with respect to $\tilde{z}$ and its derivative.

Assumption 3 (*Zhang et al., 2021; Chu et al., 2017*). D is assumed to be bounded and satisfies $|D| \leq D_0$ where D_0 is an unknown positive upper bound.

Remark 6. Recalling Assumption 1 and Remarks 3–5, one has $\frac{d+\rho(u)}{\boldsymbol{\Gamma}^T(u)\boldsymbol{\Phi}(u)}$ is bounded, which indicates that if the control input u_c is constrained, the boundedness of Assumption 3 will be guaranteed.

To satisfy the condition $s\dot{s} \leq -k_D|s|$, it is straightforward to choose an ideal control law as

$$u_c = -F - D - k_D\mathrm{sgn}(s) \tag{24}$$

where k_D is a positive constant and $\mathrm{sgn}(\cdot)$ is a sign function.

Since F and D are unknown as mentioned in Remark 5, (24) is impossible in practice. Before introducing the final adaptive bounded depth control law, two preparations are required. Firstly, for the unknown continuous function F, there exists an optimal system based on fuzzy universal approximation theorem such that

$$F = \boldsymbol{\Theta}^T\boldsymbol{\Xi} + \epsilon \tag{25}$$

where $\boldsymbol{\Theta} = [\theta_1, \theta_2, \ldots, \theta_m]^\top$ is the parameter vector, $\boldsymbol{\Xi} = [\xi_1, \xi_2, \ldots, \xi_m]^\top$ is the regressive vector, and ϵ is the fuzzy approximation error.

Assumption 4 (*Shojaei and Chatraei, 2021; Yu et al., 2020*). The approximation error ϵ is bounded and satisfies $|\epsilon| \leq D_1$ where D_1 is an unknown positive upper bound.

Secondly, rather than driving the discontinues control law with the sliding surface s in (24), a tuning error s_ε is introduced as follows

$$s_\varepsilon = s - \varepsilon\mathrm{sat}(\frac{s}{\varepsilon}) \tag{26}$$

where ε is an arbitrary positive constant to be designed and $\mathrm{sat}(\frac{s}{\varepsilon})$ is a saturation function defined by

$$\mathrm{sat}(\frac{s}{\varepsilon}) = \begin{cases}1, & \text{for } s \geq \varepsilon, \\ \frac{s}{\varepsilon}, & \text{for } -\varepsilon < s < \varepsilon, \\ -1, & \text{for } s \leq -\varepsilon,\end{cases} \tag{27}$$

Based on the above two preparations, the following adaptive bounded depth control law is proposed

$$u_{c0} = -\hat{\boldsymbol{\Theta}}^T\boldsymbol{\Xi} - \hat{D}_m\mathrm{sat}(\frac{s}{\varepsilon}) \tag{28}$$

with

$$\dot{\hat{\boldsymbol{\Theta}}} = \begin{cases}s_\varepsilon\gamma\boldsymbol{\Xi}, & \text{for } \hat{\boldsymbol{\Theta}} \in S_0 \text{ or } \hat{\boldsymbol{\Theta}} \in \delta(S) \text{ and } s_\varepsilon\boldsymbol{\Xi}^T\hat{\boldsymbol{\Theta}} \leq 0, \\ (\boldsymbol{I} - \frac{\hat{\boldsymbol{\Theta}}\hat{\boldsymbol{\Theta}}^T}{\hat{\boldsymbol{\Theta}}^T\hat{\boldsymbol{\Theta}}})s_\varepsilon\gamma\boldsymbol{\Xi}, & \text{otherwise},\end{cases} \tag{29}$$

and

$$\dot{\hat{D}}_m = \begin{cases}\kappa|s_\varepsilon|, & \text{for } \hat{D}_m < \Omega_2 \text{ or } \hat{D}_m = \Omega_2 \text{ and } |s_\varepsilon|\hat{D}_m \leq 0, \\ 0, & \text{otherwise},\end{cases} \tag{30}$$

where $\hat{\boldsymbol{\Theta}}$ is the estimate of $\boldsymbol{\Theta}$, $\hat{D}_m$ is the estimate of D_m with $D_m = D_0 + D_1$, $S_0 = \{\hat{\boldsymbol{\Theta}} \in R^n | \|\hat{\boldsymbol{\Theta}}\|_2 < \Omega_1\}$, $\delta(S) = \{\hat{\boldsymbol{\Theta}} \in R^n | \|\hat{\boldsymbol{\Theta}}\|_2 = \Omega_1\}$, Ω_i is a constant, and γ and κ are positive control gains. It can be noted that gradient projection method is resorted to guarantee the boundedness of u_c.

Although u_{c0} in (28) is always changing in $[-\Omega_1 - \Omega_2 - \rho, \Omega_1 + \Omega_2 + \rho]$ with ρ being a very small positive constant, it is likely to fall into the dead-zone region $[u_r, u_l]$. It is well known that the dead-zone breakpoints u_r and u_l can be easily obtained by experiments in advance. Therefore, if breakpoints can be moved to the origin of coordinate, the output command of the designed controller could avoid the dead-zone phenomenon. Hence, the final depth tracking control law u_c after the translation compensation for thruster's dead-zone is updated as

$$u_c = \begin{cases}u_{c0} + u_r, & \text{for } u_{c0} \geq 0, \\ u_{c0} + u_l, & \text{for } u_{c0} < 0,\end{cases} \tag{31}$$

Remark 7. Recalling (28), it has the following inequality $u_c \in [-\Omega_1 - \Omega_2 + u_l - \rho, u_l] \bigcup [u_r, \Omega_1 + \Omega_2 + u_r + \rho]$. Therefore, we can control the output command of the designed adaptive bounded depth controller to locate in the permitted range that neither falls into dead-zone nor reaches the maximum/minimum value.

3.2. Stability analysis

To establish global stability, we define a positive Lyapunov candidate function with respect to all the errors as

$$V = \frac{1}{2K}s_\varepsilon^2 + \frac{1}{2\gamma}\tilde{\boldsymbol{\Theta}}^T\tilde{\boldsymbol{\Theta}} + \frac{1}{2\kappa}\tilde{D}_m^2 \tag{32}$$

where $K = \frac{\boldsymbol{\Gamma}^T(u)\boldsymbol{\Phi}(u)}{\alpha m_{33}} > 0$, $\tilde{\boldsymbol{\Theta}} = \hat{\boldsymbol{\Theta}} - \boldsymbol{\Theta}$, and $\tilde{D}_m = \hat{D}_m - D_m$.

Differentiating (32) with respect to t yields

$$\dot{V} = -\frac{\dot{K}}{2K^2}s_\varepsilon^2 + \frac{1}{K}s_\varepsilon\dot{s}_\varepsilon + \frac{1}{\gamma}\tilde{\boldsymbol{\Theta}}^T\dot{\hat{\boldsymbol{\Theta}}} + \frac{1}{\kappa}\tilde{D}_m\dot{\hat{D}}_m \tag{33}$$

Recalling (23), Assumption 2, and Remark 5, it follows that

$$\dot{K} = \frac{1}{\alpha m_{33}} \begin{cases} \dot{\tau}_{cr}(u), & \text{for } u \geq u_l, \\ \dot{\tau}_{cl}(u) + \dot{\tau}_{cr}(u), & \text{for } u_r < u < u_l, \\ \dot{\tau}_{cl}(u), & \text{for } u \leq u_r, \end{cases} \tag{34}$$

is positive and then the first term in (33) is negative.

Resorting to (26) and $s_\varepsilon = 0$ for $-\varepsilon < s < \varepsilon$, the second term in (33) can be rewritten as

$$\begin{aligned} s_\varepsilon \dot{s}_\varepsilon &= s_\varepsilon [\dot{s} - \varepsilon \dot{\text{sat}}(\frac{s}{\varepsilon})] \\ &= s_\varepsilon \dot{s} - \begin{cases} s_\varepsilon \varepsilon \times 0, & \text{for } s \geq \varepsilon \\ 0 \times \dot{s}, & \text{for } -\varepsilon < s < \varepsilon \\ s_\varepsilon \varepsilon \times 0, & \text{for } s \leq -\varepsilon \end{cases} \\ &= s_\varepsilon \dot{s} \end{aligned} \tag{35}$$

Substituting (28) into (23) leads to

$$\dot{s} = K[-\tilde{\boldsymbol{\Theta}}^T \boldsymbol{\Xi} + \epsilon + D - \hat{D}_m \text{sat}(\frac{s}{\varepsilon})] \tag{36}$$

In terms of (29), (30), (34)–(36), (33) becomes

$$\begin{aligned} \dot{V} &= -\frac{\dot{K}}{2K^2} s_\varepsilon^2 + s_\varepsilon [-\tilde{\boldsymbol{\Theta}}^T \boldsymbol{\Xi} + \epsilon + D - \hat{D}_m \text{sat}(\frac{s}{\varepsilon})] + \frac{1}{\gamma} \tilde{\boldsymbol{\Theta}}^T \dot{\hat{\boldsymbol{\Theta}}} + \frac{1}{\kappa} \tilde{D}_m \dot{\hat{D}}_m \\ &= -\frac{\dot{K}}{2K^2} s_\varepsilon^2 - s_\varepsilon \tilde{\boldsymbol{\Theta}}^T \boldsymbol{\Xi} + \frac{1}{\gamma} \tilde{\boldsymbol{\Theta}}^T \dot{\hat{\boldsymbol{\Theta}}} - s_\varepsilon \hat{D}_m \text{sat}(\frac{s}{\varepsilon}) + \frac{1}{\kappa} \tilde{D}_m \dot{\hat{D}}_m + s_\varepsilon (\epsilon + D) \\ &= -\frac{\dot{K}}{2K^2} s_\varepsilon^2 - s_\varepsilon \hat{D}_m \text{sat}(\frac{s}{\varepsilon}) + (\hat{D}_m - D_m)|s_\varepsilon| + s_\varepsilon (\epsilon + D) \end{aligned} \tag{37}$$

Since

$$\begin{aligned} s_\varepsilon \text{sat}(\frac{s}{\varepsilon}) &= \begin{cases} s_\varepsilon \times 1, & \text{for } s \geq \varepsilon \\ 0 \times \frac{s}{\varepsilon}, & \text{for } -\varepsilon < s < \varepsilon \\ s_\varepsilon \times (-1), & \text{for } s \leq -\varepsilon \end{cases} \\ &= |s_\varepsilon| \end{aligned} \tag{38}$$

we can rewritten (37) as

$$\begin{aligned} \dot{V} &= -\frac{\dot{K}}{2K^2} s_\varepsilon^2 - \hat{D}_m |s_\varepsilon| + (\hat{D}_m - D_m)|s_\varepsilon| + s_\varepsilon (\epsilon + D) \\ &= -\frac{\dot{K}}{2K^2} s_\varepsilon^2 - D_m |s_\varepsilon| + s_\varepsilon (\epsilon + D) \\ &\leq -\frac{\dot{K}}{2K^2} s_\varepsilon^2 \end{aligned} \tag{39}$$

Integrating both sides of (39) yields that

$$\int_0^t \frac{\dot{K}}{2K^2} s_\varepsilon^2(\tau) d\tau \leq V(0) - V(\infty) < \infty, \forall t \geq 0 \tag{40}$$

Furthermore, $s_\varepsilon \dot{s}_\varepsilon$ is bounded by combining (35) and (36). From Barbalat lemma, it follows that $s_\varepsilon(t) \to 0$ as $t \to \infty$. Therefore, it can be concluded that $|\tilde{z}(t)| \leq \frac{1}{\lambda^2}\varepsilon$ as $t \to \infty$ referring to Wang et al. (2004).

4. Experimental study

4.1. Experimental platform

In order to verify the effectiveness and performance of the designed adaptive bounded controller for depth tracking of underwater vehicles, the above algorithms defined by Eqs. (28)–(32) are programmed and implemented on an STM32F429IGT6-based controller of a small-scale underwater vehicle prototype, as shown in Fig. 4. The onboard controller obtains the current depth information of the underwater vehicle by the depth gauge of MS5837, calculates the control command based on the adaptive bounded law, and then sends it to the brushless DC motor (ROVMAKER-2216) to drive the vehicle converging to the desired depth. In addition, a wireless data transmission module (YL-100) is put behind the onboard controller to comminute with the surface monitoring platform at 2 Hz. This vehicle measures approximately 0.48 m long and 0.16 m wide, and it weighs approximately 7.1 kg in air and has a small positive buoyancy in water. For this underwater vehicle, the rotation speed of the underwater thruster is adjusted by pulse width modulation (PWM). Its dead-zone and saturation parameters are set as $u_l = -40\,\mu s$, $u_r = 7\,\mu s$, $u_{cl} = -65.5\,\mu s$, and $u_{cr} = 32.5\,\mu s$, which are high level increments relative to the zero point (1500 μs). In addition, all the control gains are chosen by the trial-and-error method and are given as follows: $\lambda = 0.6, \gamma = 0.01, \kappa = 0.1, \varepsilon = 0.1$.

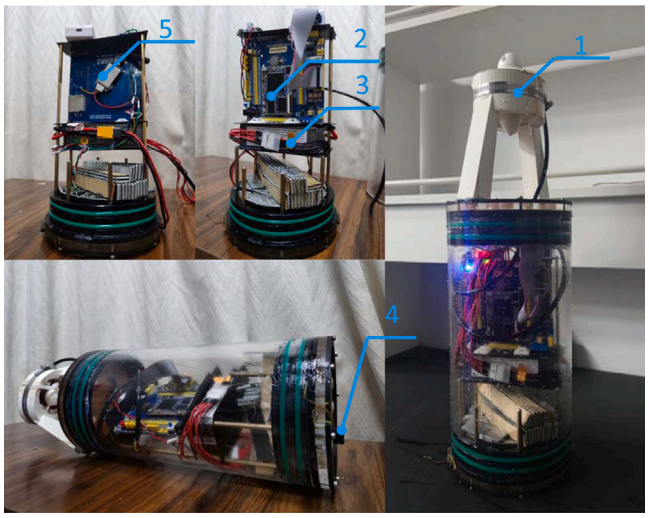

Fig. 4. Small-scale underwater vehicle testing platform (1—Thruster; 2—Controller; 3—Battery; 4—Depth gauge; 5—Wireless data transmission module).

Three groups of experiments are subsequently scheduled and carried out in an indoor water tank: the first group (*Section* 4.2) shows adaptive bounded depth tracking differences with and without thruster's dead-zone compensation; the second group (*Section* 4.3) gives the comparative results between the designed adaptive bounded controller (ABC) and the classical PID controller; and the last group (*Section* 4.4) highlights the performance of ABC against different initial tracking errors. All the results support that the designed adaptive bounded depth tracking controller has good performance in terms of accuracy, stability and adaptability. Yet, its rapidity of convergence and energy consumption can be further improved.

4.2. Comparison of the adaptive bounded depth tracking controller with /without dead-zone compensation

In this experiment, the vehicle is required to track a depth profile of 0.65 m while its current depth is 0.5 m. Two kinds of controllers including ABC with dead-zone compensation (wic) and ABC without dead-zone compensation (woc) are tested, separately. The corresponding depth tracking curves are depicted in Fig. 5, where the green one denotes the depth curve without dead-zone compensation and the black one is the depth curve with dead-zone compensation. In order to compare them in details, the whole depth tracking error $\tilde{z}$ and the intermediate depth tuning error s_ε that ABC uses are then drawn in Fig. 6. Obviously, introducing dead-zone compensation makes two depth errors fluctuate within a more narrow range. That may be because if thruster's command falls into dead-zone region, the actual effective thrust without dead-zone compensation will be zero, resulting in a thrust reduction. However, the proposed ABC with dead-zone compensation generates a nonzero value and this compensation is persistent in the entire command region. Moreover, more comparison is given in Table 1, which indicates that more precise and stable tracking performance is attributed to the compensation for thruster's dead-zone.

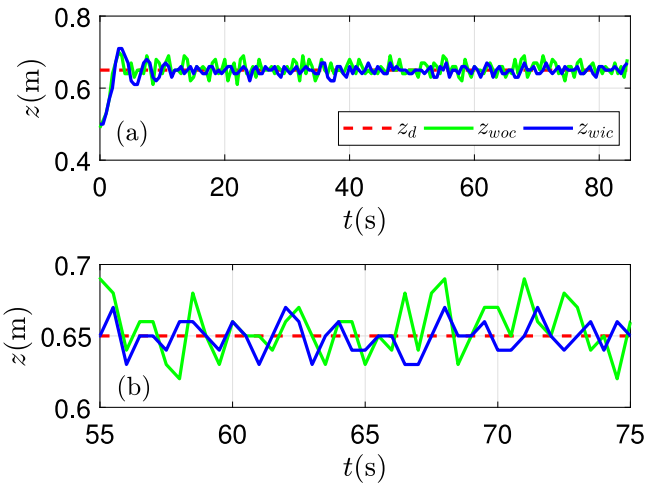

Fig. 5. Depth tracking curves with/without dead-zone compensation (a) $t = [0 - 85]$ s; (b) $t = [55 - 75]$ s. (For interpretation of the references to color in this figure legend, the reader is referred to the web version of this article.)

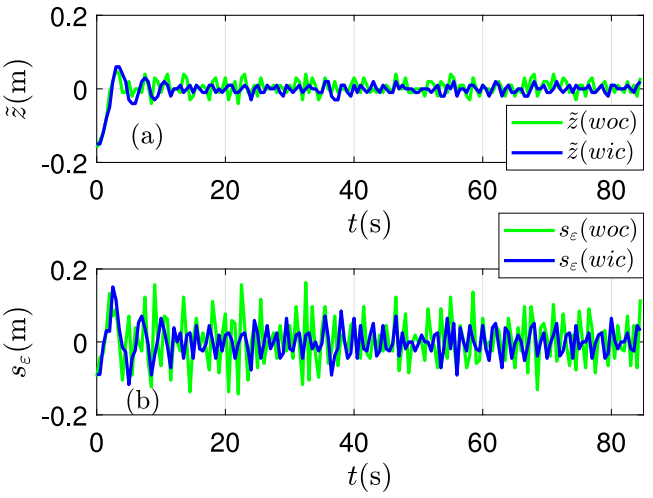

Fig. 6. Depth tracking errors (a) and tuning errors (b) with/without dead-zone compensation.

Table 1
Comparison details of depth tracking errors with/without dead-zone compensation (IA: integrated absolute; RMSE: root mean square error).

Method	Overshot/× 10^{-2} m	Rise time/s	IA/m	RMSE/× 10^{-2} m
ABC(woc)	5	2.5	3.04	2.7589
ABC(wic)	6	2.5	2.28	2.4781

In the experiment, the thruster command is also recorded and depicted in Figs. 7 and 8 in the form of scatter diagram. Notice that it is likely that the thruster command falls into dead-zone region if there is no compensation. Once it falls into dead-zone region, the actual effective action is always zero, which maybe result in a larger command to reject this reduction.

4.3. Comparison of the adaptive depth tracking controller with different controllers

In the second group of experiments, we make a comparison between the designed ABC with dead-zone compensation and the classical PID controller with dead-zone compensation in tracking the same variable-depth profile. The desired variable-depth curve includes three

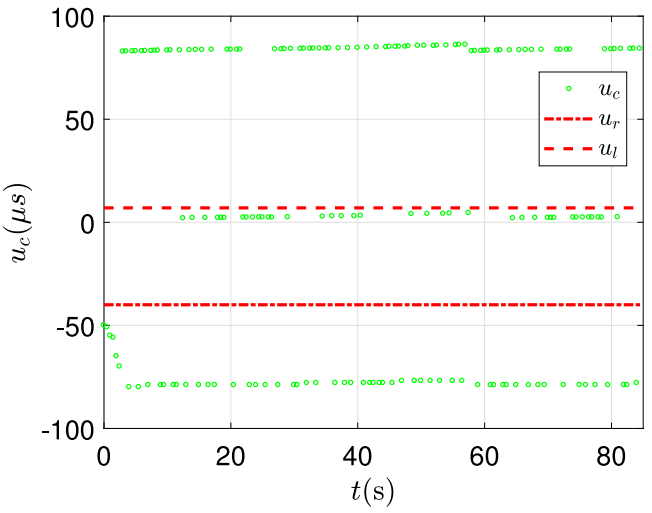

Fig. 7. Thruster command without dead-zone compensation.

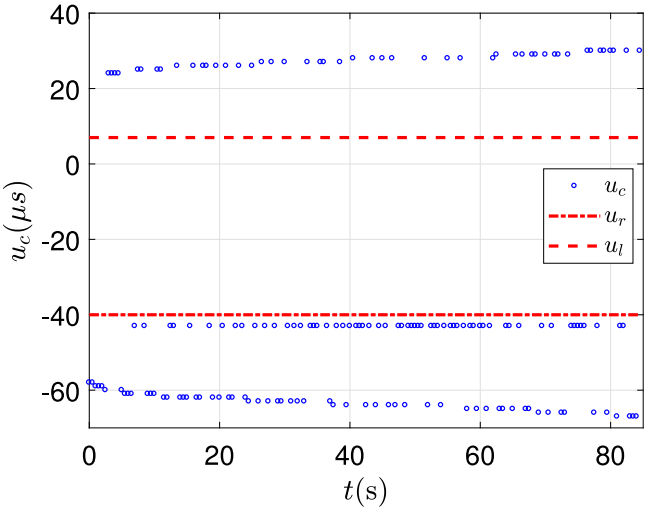

Fig. 8. Thruster command with dead-zone compensation.

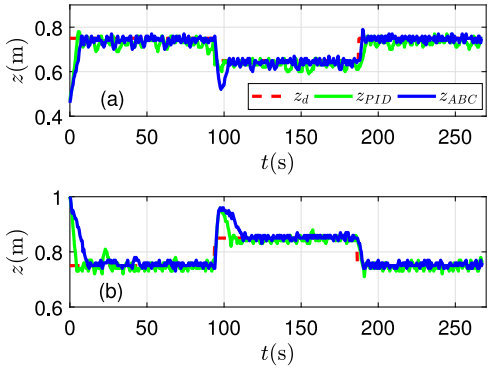

Fig. 9. Depth tracking curves under ABC and PID.

bathymetric lines. Twice experiments marked as (a) and (b) are carried out and the corresponding results are shown in Figs. 9 and 10, which describe the depth and error, respectively. More quantitative comparisons are listed in Table 2. It can be seen that the designed ABC performs better than the classical PID controller in terms of stable state errors. Yet, the former faces a energy consumption growth by

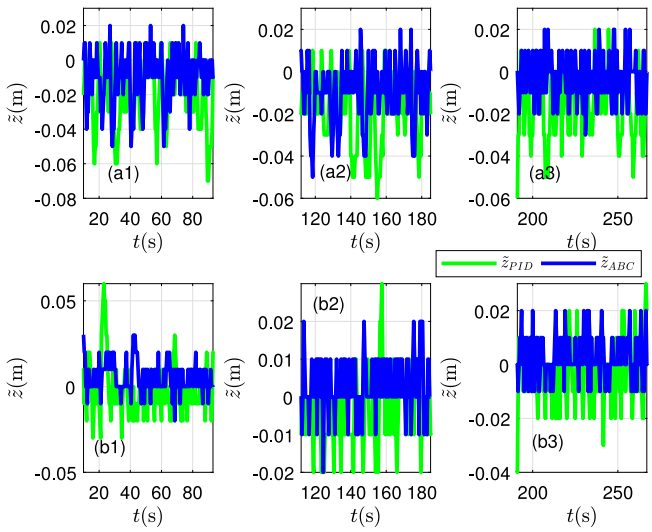

Fig. 10. Depth tracking errors under ABC and PID.

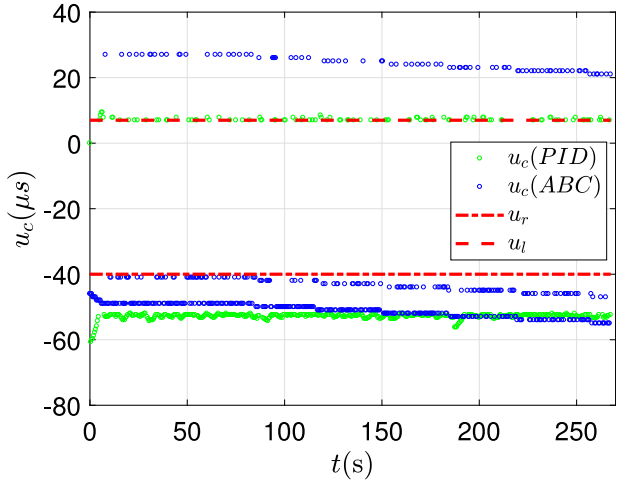

Fig. 11. Thruster command of Case (a).

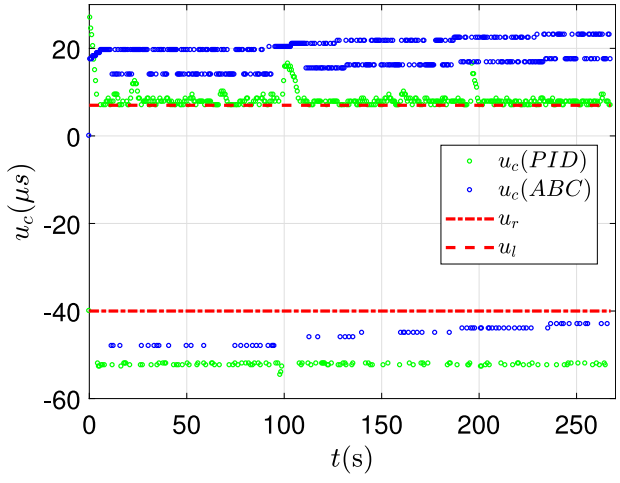

Fig. 12. Thruster command of Case (b).

0.56% and 5.84%, respectively. The command details are recorded and depicted in Figs. 11 and 12, respectively.

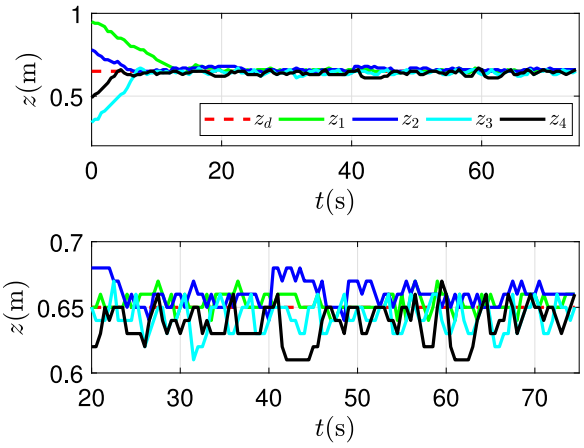

Fig. 13. Depth tracking curves with different initial errors.

Table 2
Comparison details of depth tracking errors under different controllers (T_1 = [10, 93] s; T_2 = [112, 185] s; T_3 = [191, 267] s).

Controller	Overshot(T_1; T_2; T_3)/× 10^{-2} m	IA(T_1; T_2; T_3)/× 10^{-2} m	RMSE(T_1; T_2; T_3)/× 10^{-2} m
(a)PID	3;−2;1	367;299;278	2.5607;2.4484;2.2798
(a)ABC	1;−13;4	231;195;129	1.7093;1.7378;1.1384
(b)PID	−2;11;−4	182;113;124	1.4105;1.2570;1.1355
(b)ABC	−1;11;−1	168;89;95	1.8143;1.1402;0.8773

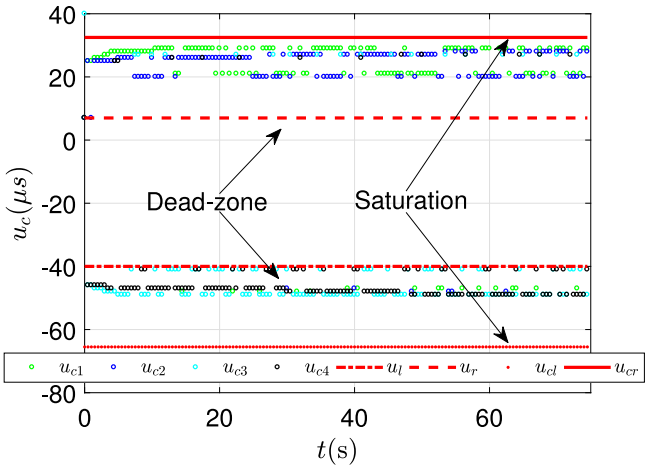

Fig. 14. Thruster's commands with different initial errors.

4.4. Comparison of the adaptive bounded depth tracking controller against different initial errors

In the last experiment, we test the performance of the designed ABC with the same control parameters against different initial depth errors. The desired depth line is set as 0.65 m, and four different initial errors are chosen as 0.3 m, 0.13 m, −0.31 m, and −0.16 m, respectively. Although the same control parameters are applied to the designed ABC, different initial errors can converge to a small range around ±0.04 m region, as shown in Fig. 13. All the thruster's commands outputted by the designed ABC with dead-zone compensation are given in Fig. 14 and they change within the permitted range.

5. Conclusions

In this paper, an adaptive bounded control law based on fuzzy universal approximation theorem, adaptive sliding mode technique, gradient projection method, and translation compensation is proposed to achieve depth tracking control for an underwater vehicle. Theoretical analysis indicates that the above controller is bound and stable. Final experiments illustrate the designed depth tracking controller has a better stable state tracking accuracy in the presence of thruster's dead-zone and saturation. In the future, we will upgrade onboard equipment and focus on experimental validation of a higher frequency and more degrees-of-freedom coupled tracking control for underwater vehicles.

CRediT authorship contribution statement

Caoyang Yu: Conceptualization, Methodology, Investigation, Writing – original draft, Writing - review & editing. **Yiming Zhong:** Software, Validation, Formal analysis. **Lian Lian:** Supervision, Funding acquisition. **Xianbo Xiang:** Supervision.

Declaration of competing interest

The authors declare that they have no known competing financial interests or personal relationships that could have appeared to influence the work reported in this paper.

Acknowledgment

This work was supported in part by the National Natural Science Foundation of China under Grants 51909161 and 52071153, in part by the Shanghai Sailing Program under Grant 19YF1424100, in part by the Open Research Fund of Key Laboratory of Marine Environmental Survey Technology and Application, Ministry of Natural Resources under Grant MESTA-2020-B008, in part by the Open Research Fund of State Key Laboratory of Ocean Engineering, Shanghai Jiao Tong University, China under Grant 1914, in part by the Startup Fund for Youngman Research at Shanghai Jiao Tong University, China under Grant 19X100040001, and in part by the Key Prospective Research Fund of Shanghai Jiao Tong University, China under Grant 2020QY10.

References

Chen, Y., Wang, K., Chen, W., 2019. Adaptive fuzzy depth control with trajectory feedforward compensator for autonomous underwater vehicles. Adv. Mech. Eng. 11 (3), 168781401983817.

Chu, Z., Xiang, X., Zhu, D., Luo, C., Xie, D., 2018. Adaptive fuzzy sliding mode diving control for autonomous underwater vehicle with input constraint. Int. J. Fuzzy Syst. 20 (5), 1460–1469.

Chu, Z., Zhu, D., Yang, S.X., Jan, G.E., 2017. Adaptive sliding mode control for depth trajectory tracking of remotely operated vehicle with thruster nonlinearity. J. Navig. 70 (1), 149–164.

Cui, R., Yang, C., Li, Y., Sharma, S., 2017. Adaptive neural network control of AUVs with control input nonlinearities using reinforcement learning. IEEE Trans. Syst. Man Cybern. Syst. 47 (6), 1019–1029.

Do, K.D., 2016. Global robust adaptive path-tracking control of underactuated ships under stochastic disturbances. Ocean Eng. 111, 267–278.

Fossen, T.I., 1994. Guidance and Control of Ocean Vehicles. Wiley New York.

Fossen, T.I., 2011. Handbook of Marine Craft Hydrodynamics and Motion Control. Wiley.

Fossen, T.I., Berge, S.P., Nonlinear vectorial backstepping design for global exponential tracking of marine vessels in the presence of actuator dynamics, in: Proceedings of the 36th IEEE Conference on Decision and Control, 1997. pp. 4237–4242.

Healey, A.J., Lienard, D., 1993. Multivariable sliding mode control for autonomous diving and steering of unmanned underwater vehicles. IEEE J. Ocean. Eng. 18 (3), 327–339.

Lakhekar, G.V., Waghmare, L.M., Jadhav, P.G., Roy, R.G., 2020. Robust diving motion control of an autonomous underwater vehicle using adaptive neuro-fuzzy sliding mode technique. IEEE Access 8, 109891–109904.

Lapierre, L., 2009. Robust diving control of an AUV. Ocean Eng. 36 (1), 92–104.

Li, D.J., Chen, Y.H., Shi, J.G., Yang, C.J., 2015. Autonomous underwater vehicle docking system for cabled ocean observatory network. Ocean Eng. 109 (15), 127–134.

Maalouf, D., Chemori, A., Creuze, V., 2015. L1 adaptive depth and pitch control of an underwater vehicle with real-time experiments. Ocean Eng. 98, 66–77.

Naik, M.S., Singh, S.N., 2007. State-dependent riccati equation-based robust dive plane control of AUV with control constraints. Ocean Eng. 34 (11), 1711–1723.

Peng, Z., Wang, J., 2018. Output-feedback path-following control of autonomous underwater vehicles based on an extended state observer and projection neural networks. IEEE Trans. Syst. Man Cybern. Syst. 48 (4), 535–544.

Ropars, B., Lapierre, L., Lasbouygues, A., Andreu, D., Zapata, R., 2018. Redundant actuation system of an underwater vehicle. Ocean Eng. 151, 276–289.

Sedghi, F., Arefi, M.M., Abooee, A., Kaynak, O., 2021. Adaptive robust finite-time nonlinear control of a typical autonomous underwater vehicle with saturated inputs and uncertainties. IEEE/ASME Trans. Mechatronics 26 (5), 2517–2527.

Shojaei, K., Chatraei, A., 2021. Robust platoon control of underactuated autonomous underwater vehicles subjected to nonlinearities, uncertainties and range and angle constraints. Appl. Ocean Res. 110, 102594.

Solowjow, E., Lange, J., Pick, M.A., Bessa, W.M., Kreuzer, E., 2017. Design and adaptive depth control of a micro diving agent. IEEE Robot. Autom. Lett. 1871–1877.

Tanakitkorn, K., Wilson, P.A., Turnock, S.R., Phillips, A.B., 2017. Depth control for an over-actuated, hover-capable autonomous underwater vehicle with experimental verification. Mechatronics 41, 67–81.

Wang, N., Li, H., 2020. Leader-follower formation control of surface vehicles: A fixed-time control approach. ISA Trans. http://dx.doi.org/10.1016/j.isatra.2020.05.042.

Wang, X., Su, C., Hong, H., 2004. Robust adaptive control of a class of nonlinear systems with unknown dead-zone. Automatica 40 (3), 407–413.

Wang, Z., Yang, S., Xiang, X., Vasilijevic, A., Miskovic, N., Nad, D., 2021. Cloud-based mission control of USv fleet: Architecture, implementation and experiments. Control Eng. Pract. 106, 104657.

Wu, N., Wu, C., Ge, T., Yang, D., Yang, R., 2018. Pitch channel control of a REMUS AUV with input saturation and coupling disturbances. Appl. Sci. 8 (2), 253.

Xia, G., Pang, C., Xue, J., 2015. Fuzzy neural network-based robust adaptive control for dynamic positioning of underwater vehicles with input dead-zone. J. Intell. Fuzzy Systems 29 (6), 2585–2595.

Yu, C., Xiang, X., Wilson, P.A., Zhang, Q., 2020. Guidance-error-based robust fuzzy adaptive control for bottom following of a flight-style AUV with saturated actuator dynamics. IEEE Trans. Cybern. 50 (5), 1887–1899.

Yu, C., Xiang, X., Zhang, Q., Xu, G., 2018. Adaptive fuzzy trajectory tracking control of an under-actuated autonomous underwater vehicle subject to actuator saturation. Int. J. Fuzzy Syst. 20 (1), 269–279.

Zhang, J., Xiang, X., Lapierre, L., Zhang, Q., Li, W., 2021. Approach-angle-based three-dimensional indirect adaptive fuzzy path following of under-actuated AUV with input saturation. Appl. Ocean Res. 107, 102486.